Flame Propagation in the Stratified Mixing Layer between CH_4 and CO_2/O_2 Stream

Chih-Yung Wu[1], Kun-Ho Chen[2], Wan-Ching Yu[1]
Department of Mechanics and Automation, Kao Yuan University
Advanced Engine Research Center
Kaohsiung, Taiwan

[2]Advanced Engine Research Center, Kao Yuan University
Kaohsiung, Taiwan

1 Introductions

It has been shown that removing nitrogen from the oxidizer is an efficient method for CO_2 capture. Hence, the oxy-combustion concept [1] has been proposed and studied for decades. In addition, the emission of nitrogen oxide is also reduced. The oxy-combustion technique results in flue gases consisting of CO_2 and H_2O mainly, and producing a concentrated CO_2 for separation. In order to reduce the flame temperature, the CO_2 is also recirculated and mixed with oxygen for combustion. Flame propagation which is one of the significant factors controlling flame stabilization is an issue of considerable fundamental importance to combustor design and has been studied for several decades. For most of hydrocarbon flames, the triple flames play important roles of flame propagation in the various stratified mixing layer. According to our previous study [2],[3], during flame propagation, a complex combination of chemical reactions coupled with fluid dynamics during flame propagation caused by the intrinsic chemical properties of the fuel is observed. On the other hand, the triple flame of hydrogen fits the triple flame propagation theory more precisely as it propagates in vitiated coaxial flow [3]. Following the similar methodologies, the ignition of fuel and the propagation 1uubehavior of the jet flame base can be characterized based on the distribution of the isoline of the mixture fractions as well as the flame's kinetic properties and the chemical reactions. For oxy-fuel combustion concept, as methane flame propagating in O_2/CO_2 stream, is the propagation behavior of the leading point of the flame identical to that of the standard triple flame structure? Which interactions occur between combustion products at higher temperatures and what is the subsequent propagation behavior? What are the dynamics of the flame front and the chemical reactions? To further extend our previous work and address these questions, and to delineate the effect of CO_2 in the oxidizer stream on the flame propagation, the CH_4 laminar jet flame propagations in a quartz tube with O_2/CO_2 coaxial flow are numerically and experimentally investigated to delineate its burning phenomena, propagation, and flame structures. The calculated heat release rate contours, mixture fraction isopleths, distribution of radicals for propagating flames are presented. The distribution of radicals near the flame leading point is extensively compared in terms of H and OH species, as well as mass flux to clearly delineate the

Correspondence to:chihyungwu@gmail.com

flame structure near the leading edge. The radial distributions of heat release rate and significant reaction step is also compared in the present study.

2 Methodology

Similar to our previous study [2], the experimental setup is schematically shown in Fig. 1. The burner consists of a central and coaxial jet, and the fuel and oxidizer stream are modified by a well-contoured settling chamber. The diameters of the central jet and coaxial jet are 5 mm and 30 mm, respectively. A quartz tube 30 mm in diameter and 100 mm in length is attached to the exit of the burner. The fuel from the central jet operates at a fixed velocity of 1.7 m/s. The oxidizer velocity at the exit of the coaxial jet is also kept constant at 0.3 m/s. Research-grade CH_4, O_2, and CO_2 are measured by electronic mass flowmeters and mixed in a mixing chamber prior to the settling chamber. The uncertainty of the mass flowmeter for methane is ±1.0% of the full scale. The conditions for the present investigations of the fuel-O_2/CO_2 flame propagation are listed in Table 1. A high speed camera (Phantom V7.3) was used to capture the flame propagation process. To control the recording system precisely, both the camera and ignition device were triggered by a pulse/delay generator for synchronization. As the ignition device ignites the flame at the exit of quartz tube, the camera system is also triggered. The imaging frequency of the camera system is 3000 Hz, and the images were stored in built-in RAM (16GByte). The images can be transferred to a PC for further analysis via the USB interface. The flame base is then identified with digital image processing, and the flame-propagation trace can be expressed as a function of time. To numerically model the transient propagation of the fuel-O_2/CO_2 flame, the time-dependent governing equations of continuity, momentum, energy, and chemical species are solved using the commercial package CFD-ACE+ 2010.0 coupled with chemical kinetic mechanisms from GRI-Mech 3.0. The molecular transport and thermal data are obtained from the CHEMKIN package and the code then calculates the thermal conductivity and viscosity of the mixture using Wilke's formula. The uniform flow of fuel and oxidizer stream at 1.7 m/s and 0.3m/s respectively are specified at the inflow boundary of the computational domain. Fixed pressure boundary conditions are imposed on the open boundaries of the quartz tube exit. Non-slip, non-catalytic surface reaction and adiabatic conditions are applied to the quartz surface. The transport model also includes thermal diffusion to account for the species diffusion due to the temperature gradients. An axisymmetric, non-uniform staggered-grid system is used with a control volume formulation in accordance with the SIMPLEC algorithm and is schematically shown in Fig. 1(b). Noted that the flame coordinate for propagating flame is defined, and the axial origin is defined at the tip of flame leading edge. To calculate the flame propagation coupled with GRI-mech 3.0 effectively, a compromised grid was used in a grid-independence test. The total number of the grids was 61 in the radial and 428 in the axial directions for a computational domain of 15 mm×100 mm and a minimum grid spacing of 0.05 mm. The minimum grid size was placed near the axis and the fuel-oxidizer stream mixing layer and an enlarged grid size was used toward the outer boundaries. Convergence of the solution is declared when the ratio of change of the dependent variables to the maximum variables in that iteration is less than 1×10^{-4}.

3 Results and Discussions

Selected photographs of the flame #1 and #2 are shown in Figure 2. According to these photographs which are captured by high speed camera, the difference in the flame structures and propagation traces for the different oxidizer composition can be identified. The calculated temporal propagation traces along with the measured data are shown in Figure 3. To objectively validate the computed results with the measured data, the origin is defined as the point at which the reaction zone reaches the axial location x = 80 mm. The validation procedures are similar to those in our previous study [2], [3]. In spite of a slight under-prediction of the flame propagation traces, the experimental results still show that there is good agreement between the measured and computed results for the two flame cases.

The calculated heat release rate for flames #1 and #2 is shown in Figure 4. For flame #1, the three red lines represent the equivalence ratio equal to 0.5, 1.0 and 2.0. The isoline is plotted based on mixture fractions. Dissimilar to the standard triple flame, only rich-branch and lean branch is clearly found. In order to further identify the flame base structure, the radial distribution of heat release rate at $\bar{x}$ = 3 mm for flame #1 and #2 as the flame reaches x = 50 mm are shown in Figure 5. In addition, the computed distribution of the heat release rate along the isopleths of equivalence ratio φ = 0.5, 1.0, and 2.0 for flames #1 and #2 are shown in Figure 6. These results imply that the heat release region is concentrated near the flame leading edge and the leading point. As shown in Figure 7, both H and OH are generated in the reaction zone and play an important role in inducing methane pyrolysis by upstream diffusion. As the concentration of oxygen is increased in the oxidizer stream, more H and OH are produced to initiate fuel dissociation reactions. Figure 8 shows the radial distribution of reaction rate of R99 (OH + CO↔H + CO_2) at $\bar{x}$ = 3 mm (flame coordinate) for flame #1 and #2 as the flame reaches x = 50 mm. The results show that the reaction rate of R99 is negative in the rich-premixed reaction zone. CO is a major intermediate of hydrocarbon flames and reacts with OH through OH + CO↔H + CO_2. For the methane flame propagating in O_2/CO_2 stream, CO_2 can be decomposed with H atom.

4 Conclusions

The propagation phenomena of methane laminar flame in a well confined quartz tube with O_2/CO_2 are numerically and experimentally studied. Based on the distribution of the isopleths of the mixture fractions and the chemical reactions, this paper characterizes the flame base structure, and the propagation phenomena of the jet flame base.

5. Acknowledgement

This research was supported by the Ministry of Science and Technology of Taiwan under Grant numbers MOST 103-2221-E-244-005.

Table 1 Flame cases with various inlet conditions for coaxial oxidizer stream

case #	Fuel		Oxidizer stream			Mixture fraction (labeled with no.)		
	CH_4(vol%)	m/s	O_2 (vol%)	CO_2 (vol%)	m/s	1. φ = 0.5	2. φ = 1.0	3. φ = 2.0
1	100	1.7	40	60	0.3	0.0367	0.0755	0.1468
2	100	1.7	50	50	0.3	0.0500	0.0952	0.1739

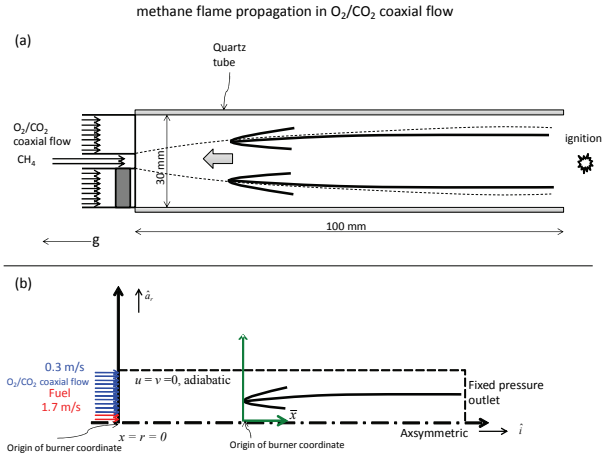

Figure 1 Schematic illusion of (a) burner, coaxial flow, confined quartz tube and the flame and (b) computational domain with boundary conditions and the coordinate systems.

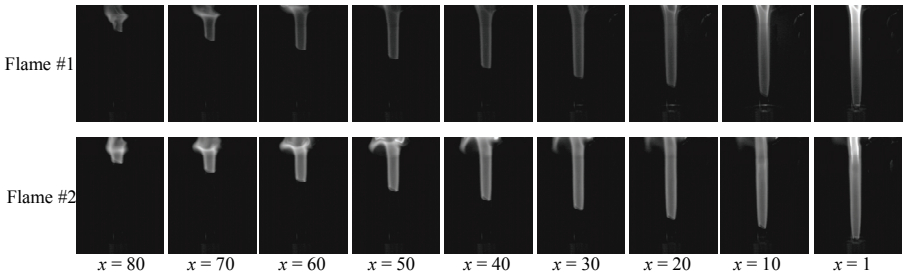

Figure 2 Photographs of the flame #1 and flame #2

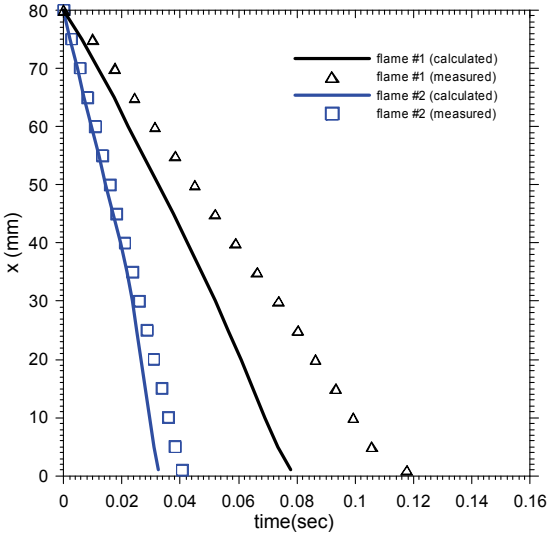

Figure 3 Calculated and measured temporal propagation flame base traces.

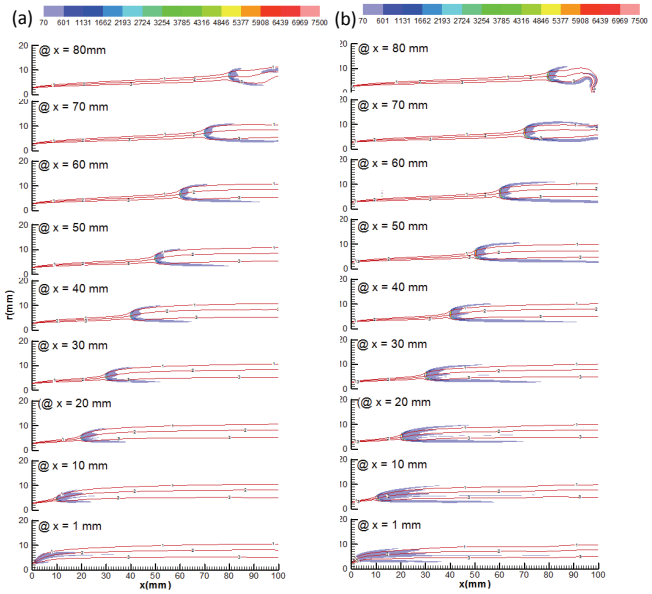

Figure 4 Flame Propagation and reaction zone in terms of heat release rate for (a) flame # 1 and (b) flame #2

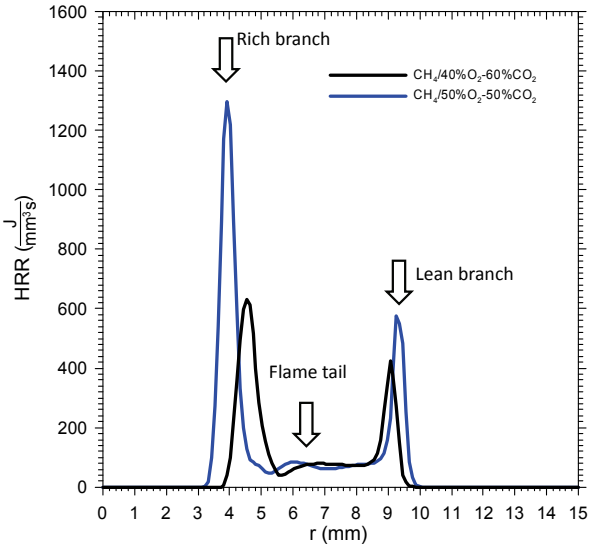

Figure 5 Radial distribution of heat release rate at $\bar{x}$ = 3 mm (flame coordinate) for flame #1 and #2 as the flame reaches x = 50 mm

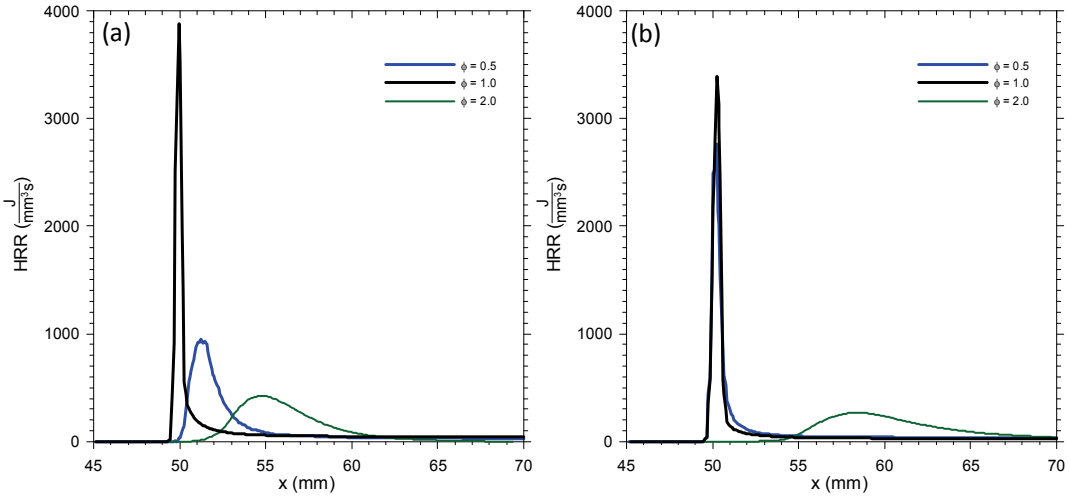

Figure 6 Computed distribution of the heat release rate along the isopleths of equivalence ratio φ = 0.5, 1.0, and 2.0 for: (a) flames #1 and (b) #2.

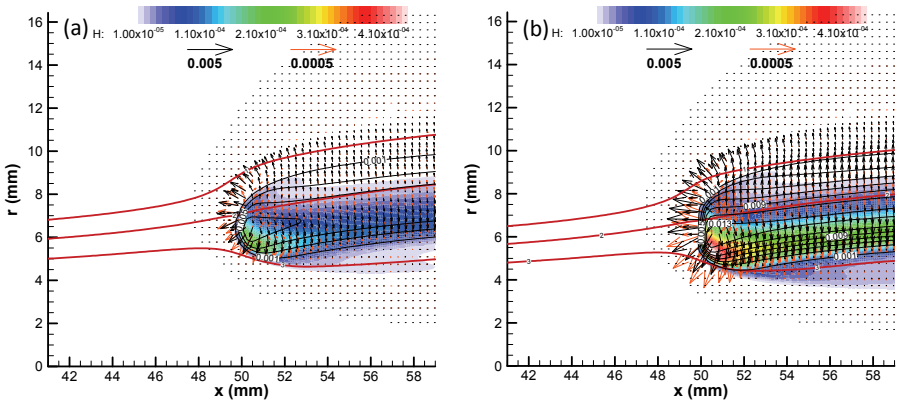

Figure 7 Flame base structure of the propagating flame for (a) flames #1 and (b) #2 in terms of calculated H contours, OH mass fraction isopleths (black), and the flux of H (orange vectors) and OH (black vectors).

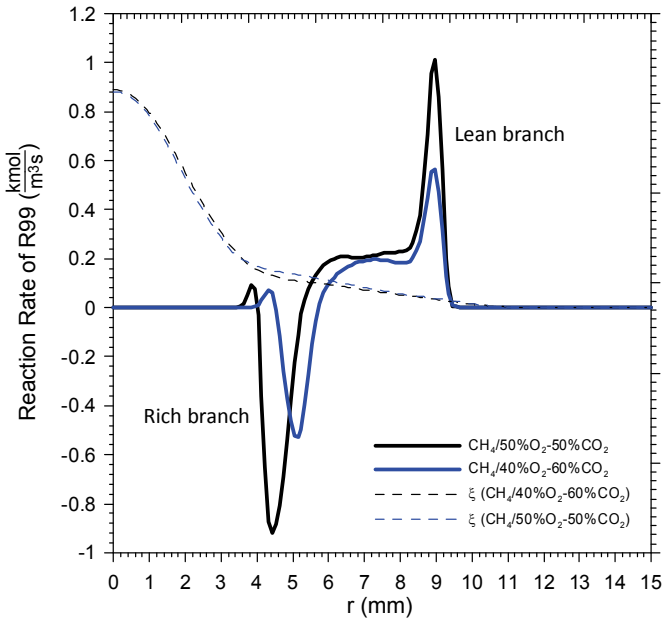

Figure 8 Radial distribution of reaction rate of OH + CO↔H + CO_2 at $\bar{x}$ = 3 mm (flame coordinate) for flame #1 and #2 as the flame reaches x = 50 mm

References

[1] Toftegaard MB, Brix J, Jensen PA, Glarborg P, Jensen AD. (2010). Oxy-fuel combustion of solid fuels. Prog. Energ. Combust. 36:581.

[2] Wu CY, Li YH, Chang TW. (2012). Effects of CO addition on the propagation characteristics of laminar CH4 triple flame. Combust. Flame. 159:2806.

[3] Wu CY, Chen KH. (2014). Characterization of hydrogen triple flame propagation in vitiated laminar coaxial flow. Int. J. Hydrogen Energ. 39:14109.